Journal of the Korean Society of Surveying, Geodesy, Photogrammetry and Cartography
Vol. 34, No. 6, 619-627, 2016
https://doi.org/10.7848/ksgpc.2016.34.6.619

ISSN 1598-4850(Print)
ISSN 2288-260X(Online)
Original article

Automatic Detection of Malfunctioning Photovoltaic Modules Using Unmanned Aerial Vehicle Thermal Infrared Images

Kim, Dusik[1)] · Youn, Junhee[2)] · Kim, Changyoon[3)]

Abstract

Cells of a PV (photovoltaic) module can suffer defects due to various causes resulting in a loss of power output. As a malfunctioning cell has a higher temperature than adjacent normal cells, it can be easily detected with a thermal infrared sensor. A conventional method of PV cell inspection is to use a hand-held infrared sensor for visual inspection. The main disadvantages of this method, when applied to a large-scale PV power plant, are that it is time-consuming and costly. This paper presents an algorithm for automatically detecting defective PV panels using images captured with a thermal imaging camera from an UAV (unmanned aerial vehicle). The proposed algorithm uses statistical analysis of thermal intensity (surface temperature) characteristics of each PV module to verify the mean intensity and standard deviation of each panel as parameters for fault diagnosis. One of the characteristics of thermal infrared imaging is that the larger the distance between sensor and target, the lower the measured temperature of the object. Consequently, a global detection rule using the mean intensity of all panels in the fault detection algorithm is not applicable. Therefore, a local detection rule was applied to automatically detect defective panels using the mean intensity and standard deviation range of each panel by array. The performance of the proposed algorithm was tested on three sample images; this verified a detection accuracy of defective panels of 97% or higher. In addition, as the proposed algorithm can adjust the range of threshold values for judging malfunction at the array level, the local detection rule is considered better suited for highly sensitive fault detection compared to a global detection rule. In this study, we used a panel area extraction method that we previously developed; fault detection accuracy would be improved if panel area extraction from images was more precise. Furthermore, the proposed algorithm contributes to the development of a maintenance and repair system for large-scale PV power plants, in combination with a geo-referencing algorithm for accurate determination of panel locations using sensor-based orientation parameters and photogrammetry from ground control points.

Keywords : Photovoltaic Module, Malfunction Panel, UAV, Infrared Thermography, Automatic Detection

1. Introduction

As a part of the Paris Agreement in December 2015, the international community agreed to “hold the increase in the global average temperature to well below 2°C” and to “pursue efforts to limit the temperature increase to 1.5°C”. This international response to climate change is scheduled to be implemented from 2020 onwards, by which time all signatories to the Paris Agreement must honor their collective commitment to curbing greenhouse gas emissions and adapting to climate change. In the years running up to this target date, they should establish energy strategies

Received 2016. 11. 28, Revised 2016. 12. 12, Accepted 2016. 12. 26
1) Member, Korea Institute of Civil Engineering and Building Technology, ICT Convergence and Integration Research Institute (E-mail: dusikkim@kict.re.kr)
2) Corresponding Author, Member, Korea Institute of Civil Engineering and Building Technology, ICT Convergence and Integration Research Institute (E-mail: younj@kict.re.kr)
3) Korea Institute of Civil Engineering and Building Technology, ICT Convergence and Integration Research Institute (E-mail: ckim@kict.re.kr)

to reduce pollution from fossil fuels, while meeting the globally increasing energy needs. In this context, South Korea identified the top 10 climate technologies with a view to developing key technologies to cope with climate change. Photovoltaic power generation is one of these 10 technologies and is emerging as a strategic technology for securing future energy for the country.

PV power generation systems have received significant attention as one of the promising renewable energy sources. However, PV panels used for collecting solar energy have an inherent disadvantage of efficiency degradation caused by the accumulation of dust or dirt as a result of their exposure to the natural environment. This leads to defects such as short circuits caused by corrosion of modules and blocking of cells. Therefore, regular inspection and constant maintenance and repair are essential for maintaining a stable power output. Visual inspection and output measurement methods can be used for fault diagnosis in PV panels with reduced output efficiency (Quater *et al*., 2014). However, given that many large-scale PV power plants will be constructed and operated in the future within the climate change response framework, large-scale PV power plant monitoring through visual inspection will be uneconomical in terms of time and expenses. For the case of the output measurement method, monitoring the output of each PV panel is a great challenge for large-scale PV power plants. Therefore, there is a need for the development of technologies to overcome the drawbacks of existing techniques.

In general, a defective cell emits thermal energy and, thus, has a higher temperature compared to the surrounding normal cells. Therefore, a thermal imaging camera can be used to efficiently detect defective spots, even during plant operation. Hand-held thermal imagers have been widely used as a conventional method for detecting defective panels as part of PV power plant inspections (Bazilian *et al*., 2002). However, the technique would be time-consuming and expensive when applied to the inspection of a large-scale PV power plant.

Recently, a PV power plant monitoring technology has been developed that uses UAVs equipped with thermal imaging cameras (Buerhop and Scheuerpflug, 2014; Grimaccia *et al*., 2015). This is a promising technology for monitoring large-scale PV power plants as it can rapidly scan a large PV array field. At the current level of technology, however, detection of defective panels is through the visual assessment of the images captured by aerial photogrammetry, and the analysis of a large number of image frames is time-consuming. This can be addressed only by developing a method for automated fault detection by combining aerial photogrammetry with computer vision technology.

Two key methods are involved in the process of the automated detection of defective panels of a PV power plant from aerial thermal infrared images. The first is the method for automatically extracting the ROI (region of interest) of a PV array field from the given images. Tsanakas *et al*. (2015) and Rogotis *et al*. (2014) presented methods for extracting the ROI from terrestrial thermal infrared image sequences using the Canny edge operator (Canny, 1986) or image segmentation techniques (Gonzalez *et al*., 2004). More recently, Kim *et al*. (2016a, 2016b) proposed an algorithm for panel area extraction from thermal infrared images captured with a UAV using the Canny edge operator and image segmentation techniques. They concluded that the area extraction method using the Canny edge operator did not lend itself well to creating a single polygon for the panel area due to noise within and outside the panels. In contrast, the image segmentation-based area extraction method was able to create polygons for individual panel areas, albeit limited by imperfect linearity. As such, while previous studies have not yet achieved optimal implementation of automated area extraction, they have demonstrated the possibility of developing automated panel area extraction, if improved computer vision technology becomes available.

The second key method is the establishment of the automatic diagnosis of defective panels based on extracted PV panel areas. Tsanakas *et al*. (2015) designed a method to identify the location of hot spot cells on a PV panel using the Canny edge operator. In the PV power plant maintenance and repair regime generally applied in South Korea, any panel containing defective cells is replaced in its entirety. Hence, the algorithm should focus on diagnosing the function or malfunction of each panel rather than identifying the locations of hot spot cells within a panel. Similarly, it is not

necessary to have high resolution images that identify each cell; the outline of a PV panel and the presence or absence of hot spots are sufficient for the rapid inspection of a large-scale PV power plants using a UAV. Consequently, it is considered reasonable to employ a method for comparing the intensity characteristics of individual panel area polygons, rather than one using threshold values, such as the Canny edge operator, for developing an algorithm in this study. In a related previous study, Kim *et al*. (2016a) proposed using statistical characteristics of the thermal image intensity as parameters for panel fault diagnosis, as defective panels display different patterns of intensity compared to intact panels. Drawing on this finding, this study aims to develop an algorithm capable of automated PV panel fault diagnosis using intensity-related statistical values of each panel based on extracted panel area polygons.

2. Analysis of PV Panel Intensity Characteristics for a Thermal Infrared Image

As experimental data, we used a sample image (Fig. 1(a)) obtained from FLIR T620 thermal imaging camera mounted on a UAV, provided online by Paul Kitawa, at a size of 640×480 pixels. In a previous study (Kim *et al*., 2016b), we developed an image segmentation-based panel area extraction algorithm and created polygons for individual panel areas as shown in Fig. 1(b). The panel area extraction algorithm generates individual panel polygons by combining the background area image and the panel boundary image. Although the extracted polygons did not show perfect linearity due to noise around the panels, the study confirmed that panel areas could be expressed with 93.9% accuracy compared with visually extracted and manually digitized panel boundaries using the performance assessment method of McGlone *et al*. (2004). In Fig. 1(c), each panel is labeled with a serial number assigned to each extracted panel area polygon. Visual inspection of the labeled panels reveals that hot spots are present on a total of five panels (6, 23, 26, 64, and 66) in a string form. Analysis of the thermal characteristics of defective PV modules suggests that these hot spots are due to defective bypass diodes within the modules (Köntges *et al*., 2014; Shin *et al*., 2015).

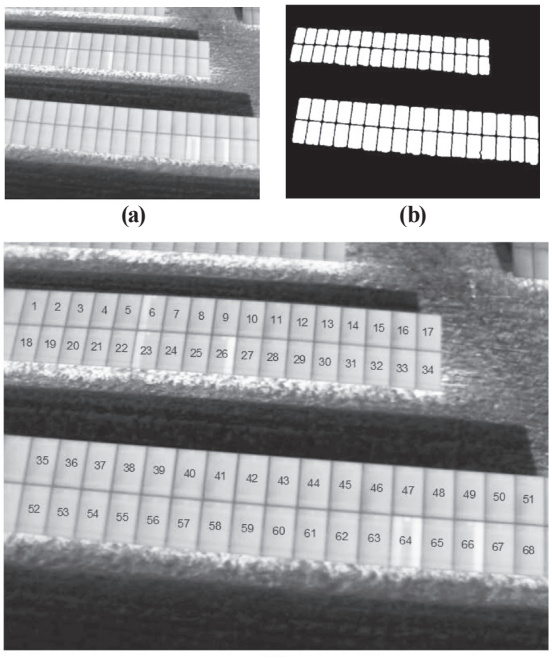

Fig. 1. (a) Sample thermal infrared image (www.kiwata.de), (b) Panel area extraction result, and (c) Gray scale image with PV module numbers labeled

Fig. 2 displays a three-dimensional (row, column, intensity) representation of the thermal intensity characteristics of the extracted panel area. Whereas most of the panels display almost the same geometry and intensity characteristics, with a very small range of variation, panels containing hot spot cells show a greater intensity of variation. The differences are too subtle to be recognized visually, however, the gray scale image clearly shows that the overall intensity of the panels increases toward the right. This may be explained by the fact that the panels situated on the right side are closer

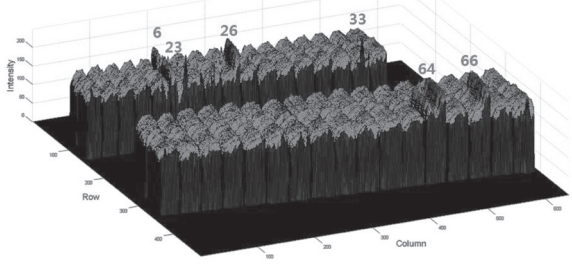

Fig. 2. Thermal intensity characteristics of the extracted panel area

to the sensor than those on the left. The high-intensity area displayed on the bottom edge of panel 33 (Fig. 2) can be attributed to imperfect panel area extraction due to noise on the ground near the panel, which caused an expanded area to be extracted on the bottom edge.

This study aims to develop an algorithm for detecting defective panels by identifying panels with hot spot cells displayed on thermal infrared images. Therefore, the algorithm should be able to identify a panel exhibiting high intensity within its ROI. In Fig. 3, the intensity range of each panel within its ROI is displayed using maximum and minimum intensity values, with blue and yellow bars representing the intensities of normal and defective panels, respectively. If a threshold method is used to diagnose defective panels, the selection of a moderate threshold (Case 1 in Fig. 3) results in many normal panels being identified as defective, in addition to those that actually are defective. When a high threshold value is set, for example in Case 2 (Fig. 3), not all defective panels are detected. In addition, if the algorithm is designed to identify defective panels merely on the basis of the maximum intensity, it is possible that a normal panel is diagnosed as being defective due to area extraction error, as in the case of panel 33. From these examples, it can be inferred that fault diagnosis based on intensity range alone is prone to error.

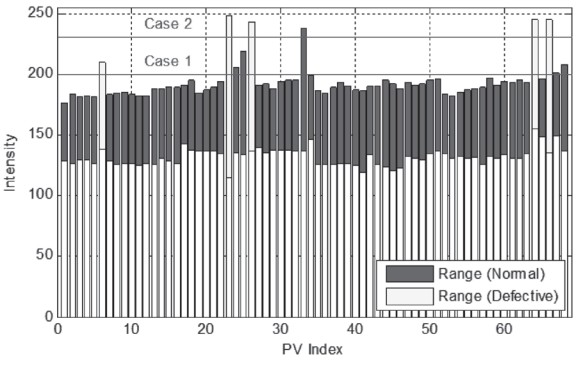

Fig. 3. Intensity range of each panel

To reduce fault diagnosis error, it is essential to consider the overall intensity characteristics of each panel. We compared intensity histograms in order to determine the intensity characteristics of normal and defective panels (Fig. 4). The histograms on the left side in Fig. 4 represent normal panels (25 and 63), and those on the right side represent defective panels (26 and 64). As intensity distributions of normal panels are similar to those of adjacent panels, normal panels close to panels with hot spots were selected for comparison. The blue solid and dotted lines in Fig. 4 represent the mean intensity and standard deviation range, respectively, of pixels in the entire panel area. The red diamond and solid line represent the mean intensity and standard deviation range, respectively, of the pixels in each panel area concerned. The normal panel histograms are distributed at an intensity range of 200 or lower and display patterns similar to the normal distribution of the entire panel area. In contrast, the defective panel histograms contain pixels with intensity values exceeding 200 and display multiple peaks that deviate from a normal distribution. Comparison of the mean intensity and standard deviation range of each panel revealed that while normal panels displayed values similar to the standard deviation range of the entire panel area, defective panels displayed higher values. This result is attributable to the increased intensity distribution range caused by the hot spots present on defective panels, resulting in a larger standard deviation.

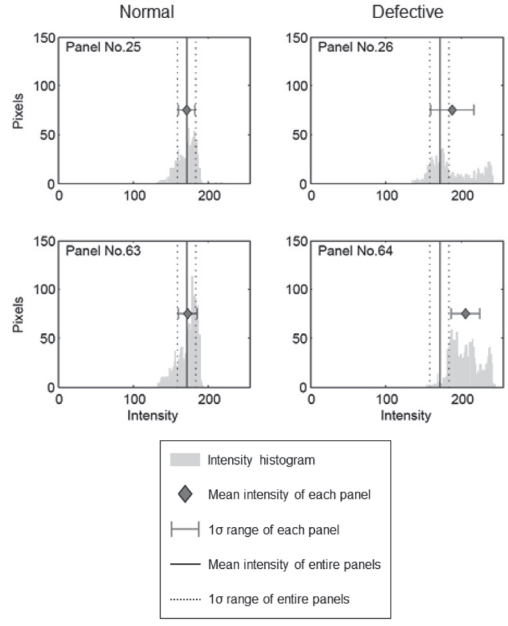

Fig. 4. Examples of the intensity histogram and statistical characteristics of normal and defective panels

The box plot (box and whisker diagram) in Fig. 5 represents the mean and standard deviation range of the intensity calculated from each of the panel area pixels. Red and green squares represent the mean intensity values of normal and defective panels, respectively, and the solid red line represents the intensity standard deviation range of each panel. As in Fig. 4, the blue solid and dotted lines represent the mean intensity and standard deviation range of pixels in the entire panel area.

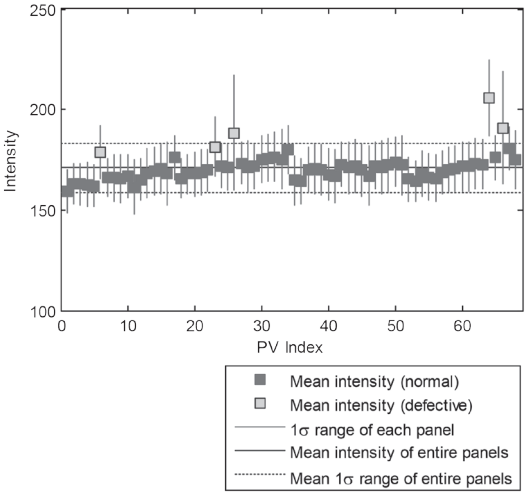

Fig. 5. Statistical characteristics of each panel

Two major characteristics can be distinguished from Fig. 5. Firstly, the mean intensity of each panel mostly falls within the standard deviation range of the mean intensity of all panels. Of the defective panels, the mean intensity of panels 26, 64, and 66 surpassed the standard deviation range of all panels, while that of panels 6 and 23 fell within it. This implies that the mean intensity of each panel is not a reliable parameter for detection of defective panels. Fortunately, the mean intensity of defective panels is substantially different from that of adjacent panels. Therefore, the mean intensity of a panel can be used as one of the inspection parameters for fault diagnosis of PV panels.

The second characteristic derived from Fig. 5 concerns the standard deviation range of each panel. When the standard deviation range of each panel was compared, defective panels showed ranges higher than those of normal panels, and above those of the entire panel dataset. In the case of panels 6 and 23, intensities at hot spot cells were lower than those of other defective panels, and close to the entire panel dataset. However, despite smaller differences, their standard deviation ranges were verified to be clearly larger than those of normal panels aligned in the same array row. Therefore, it is considered that the method of comparing with adjacent panels is more efficient for detecting defective panels than using a specific standard deviation range for diagnosis.

Application of intensity-related statistics as parameters for fault diagnosis means that detection error arising from area extraction error is precluded, which cannot be achieved using the maximum intensity for fault diagnosis. Moreover, because the method enables an automated range setting for fault diagnosis from the given images, it is judged to be adequate for the application to an automated large-scale PV power plant monitoring system.

3. Development and Evaluation of the Fault Diagnosis Algorithm

From the analysis of the intensity-related statistics, we can derive a method for assigning a reference value applicable to the fault diagnosis algorithm. For the purpose of this study, the mean intensity and standard deviation of each panel were selected as parameters for fault diagnosis of PV panels. Firstly, any panel with a mean intensity that deviates from the sample standard deviation of the sample mean intensities of the adjacent sample panels can be defined as a candidate defective panel. Here, adjacent panels are selected from panels situated in the same array. If the intensities of each panel can be normalized, the malfunction panel can be detected by analyzing the intensities of the entire panel. However, for the normalization of the intensities, parameters that can grasp the geometrical relationship between the target and the sensor are required. Since these parameters were not obtained in this study, a comparison method between adjacent panels (panels located in the same array row) was applied to detect malfunctioning panels with only sample images. As such, if the standard deviation is calculated after dividing by the number of the sample panels, the reference value for diagnosing a defective panel can be adjusted for each array, and candidate defective panels can be detected efficiently. In this study, this is defined as the CMI (criterion

for mean intensities). Next, any panel with a 1σ intensity range larger than the standard deviation (average range of samples standard deviations) of all the adjacent panels can be classified as a candidate defective panel. In this paper, this is defined as the CSD (criterion for standard deviations). Here, the average standard deviation of all the adjacent panels was calculated by assigning a weight to the number of pixels using Eq. (1), in order to reflect the different number of pixels in each panel ROI.

$$S_w = \sqrt{\frac{(n_1 - 1)S_1^2 + (n_2 - 1)S_2^2 + \cdots + (n_k - 1)S_k^2}{n_1 + n_2 + \cdots + n_k - k}} \quad (1)$$

where, S_w denotes the weighted average of standard deviations, n denotes the number of pixels of each panel, S_x the standard deviation of each panel and k the number of panels.

The conditions for defective panel detection were set as follows: (i) a mean panel intensity larger than the CMI; (ii) the sum of the average of the standard deviations and mean intensity of the target panel larger than the sum of the CMI and mean intensity. These detection conditions were selected as the purpose of this study is to detect defective panels under the assumption that panels with hot spots are defective panels. Consequently, a panel with a mean intensity lower than the CMI range on the image is considered a normal panel. This criterion setting method, which uses the 1σ range, is an empirical method derived from the thermal infrared image analysis of solar

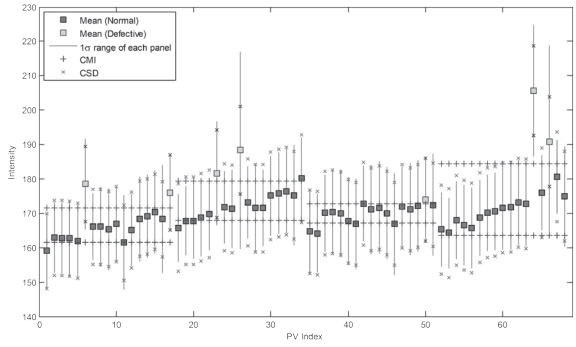

Fig. 6. Results of the fault diagnosis algorithm application

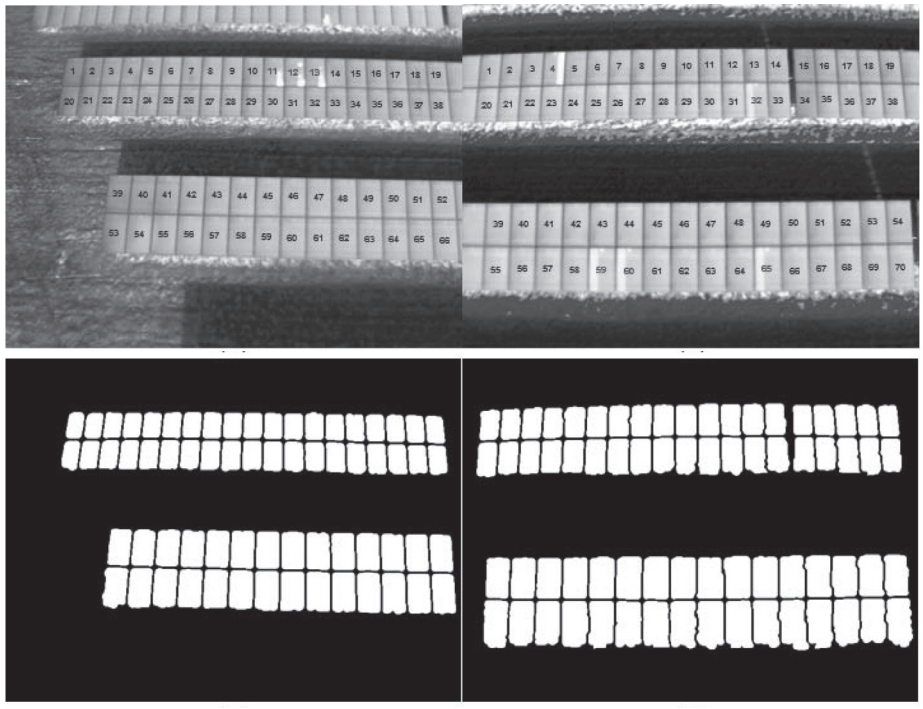

Fig. 7. (a) and (b) Additional test images for evaluation of the fault diagnosis algorithm (www.kitawa.de), (c) and (d) Results of the panel area extraction

power plants. Since this method is based on the empirical characteristics of intensity, various sample image analysis should be added to improve the integrity of the algorithm. Fig. 6 presents the results from diagnosing defective panels using the proposed algorithm. The red and green squares represent the mean intensities of the normal panels, and panels diagnosed as defective, respectively. Red lines represent the 1σ range of a given panel. Blue + and red × represent the CMI and CSD ranges, respectively. In order to show whether a panel classified as a defective panel met the CSD condition, the CSD range of the panel concerned was marked as a blue ×. Fig. 6 shows that a total of seven panels were recognized as defective, although the actual number of defective panels with hot spots on the image was confirmed as five. Hence, the algorithm was found to have limitations in fault diagnosis by classifying panels without hot spots, such as panels 17 and 50, as defective panels.

We applied the algorithm to an additional two images for evaluation purposes. Figs 7 (a) and (b) present the results of target panel labeling after converting two thermal infrared images into gray scale images. The images were retrieved from the website of Paul Kitawa, as the example image presented earlier. Drawing on our previous study (Kim *et al*., 2016b), in which panel area ROIs were generated from these images, we were able to evaluate the results of the algorithm using the images and ROI data. There are three defective panels (11, 12, and 13) on image (a) and five defective panels (4, 32, 59, 60, and 65) on image (b). Figs 7 (c) and (d) present the results of the panel area extraction.

Figs 8 and 9 represent the results of the algorithm for the images in Figs 7 (a) and (b), respectively. The results were consistent with the defective panels recognized by visual inspection, and no diagnosis error of recognizing a defective panel and a normal panel occurred. In Fig. 8, the mean intensity of each panel was found to increase exponentially as the row in the same array advanced. Likewise, the mean intensities of the normal panels generally showed a continuous pattern well-aligned with the adjacent panels in terms of mean intensity. These characteristics allowed us to conclude that it was adequate to select the mean intensity of each panel as the main parameter for fault diagnosis in the proposed algorithm.

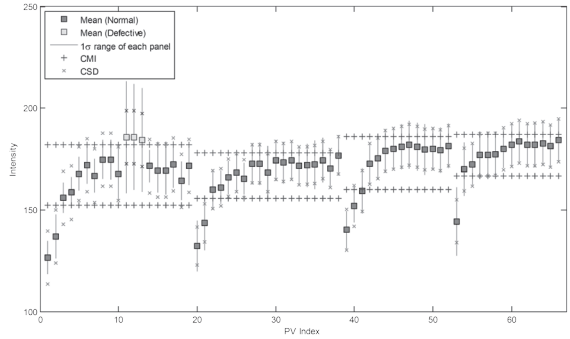

Fig. 8. Results of the algorithm implementation to the image in Fig. 7(a)

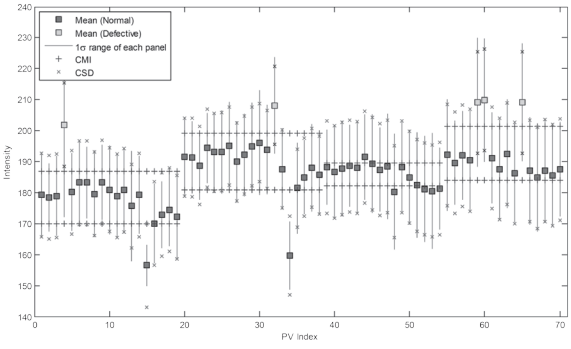

Fig. 9. Results of the algorithm implementation to the image in Fig. 7(b)

Table 1 outlines the results of the performance evaluation using a confusion matrix on the basis of the number of panels inspected. The confusion matrix is used as a method for quantitative performance evaluation of the proposed algorithm. It classifies the result of comparing the predicted class and actual class as true or false. Positive and negative values were assigned to defective and normal panels, respectively, such that values TP (True Positive), FN (False Negative), FP (False Positive), and TN (True Negative) constituting the confusion matrix were defined as follows. TP is the case where a defective panel is correctly recognized, FN is where a defective panel is not recognized, FP is where a normal panel is recognized as a defective panel, and TN is where a normal panel is not recognized. We evaluated the algorithm in terms of completeness and accuracy, with the former representing the rate of correct recognition of the defective panels displayed on the image and the later representing the degree of classification accuracy. These

two indicators were computed using Eq. (2) and Eq. (3), respectively.

$$\text{Completeness} = \frac{TP}{TP + FN} \tag{2}$$

$$\text{Accuracy} = \frac{TP + TN}{TP + FN + FP + TN} \tag{3}$$

Looking at the results presented in Table 1, FN is 0 in all three images, i.e., completeness is 100%. This means that the proposed algorithm recognized all defective panels displayed on the images. As such, this algorithm has met the purpose of detecting defective panels. However, the algorithm achieved an accuracy of approximately 97% in Fig. 1, which implies that a normal panel may be recognized as a defective panel. Therefore, it is considered necessary to improve the accuracy of the algorithm by setting out additional conditions in a future study.

Table 1. Comparison of fault detection algorithms

Image	TP	FN	FP	TN	Completeness	Accuracy
	[No. of Panels]				[%]	
Fig. 1	5	0	2	61	100	97.06
Fig. 7 (a)	3	0	0	63	100	100
Fig. 7 (b)	5	0	0	65	100	100

4. Conclusions

We developed an algorithm capable of automatically diagnosing defective PV panels based on intensity statistics. As parameters for fault diagnosis, we selected the mean intensity and standard deviation range, and applied a local detection rule to diagnose faults using the statistics of each array row, not the entire panels. In comparison with the general detection rule of computing the standard deviation of the entire data range, this method is judged to be better suited for sensitive classification as it can narrow the range of determining normal or defective panels. However, given that the proposed algorithm was implemented only on three thermal infrared images in this study, additional image analysis will have to be performed to prove the reliability of the algorithm in terms of completeness and accuracy and to further improve its performance. Additionally, the sample images were of similar panel sizes and intensity characteristics; it is thus necessary to conduct further sample analysis study, thereby varying conditions such as the years of service of panels, observation hours, and scale of photogrammetric measurement. Despite the small sample size analyzed, this study is significant in that it ascertained the feasibility of using intensity statistics of thermal infrared images as parameters for automatic fault diagnosis of PV panels. In future research, it is considered necessary to explore how to use the orientation parameters of the sensor and ground control point (GCP)-based photogrammetric surveys to precisely determine the locations of defective panels to establish an efficient maintenance and repair regimen for large-scale PV power plants

Acknowledgment

This study was conducted under the support of the project "Development of high Efficiency Solar Road Power Generation Technology" funded by the Korea Institute of Civil Engineering and Building Technology.

References

Bazilian, M.D., Kamalanathan, H., and Prasad, D.K. (2002), Thermographic analysis of a building integrated photovoltaic system, *Renewable Energy*, Vol. 26, No. 3, pp. 449-461.

Buerhop, C. and Scheuerpflug, H. (2014), Field inspection of PV-modules using aerial, drone-mounted thermography, *Proceedings of the 29th European Photovoltaic Solar Energy Conference and Exhibition (EUPVSEC)*, 22-26 September, Amsterdam, Netherlands, pp. 2975-2979.

Canny, J. (1986), A computational approach to edge detection, *IEEE Transactions on Pattern Analysis and Machine Intelligence (PAMI)*, Vol. 8, No. 6, pp. 679-698.

Gonzalez, R.C., Woods, R.E., and Eddins, S.L. (2004), *Digital Image Processing using Matlab*, Pearson Prentice Hall, N.J.

Grimaccia, F., Aghaei, M., Mussetta, M., Leva, S., and

Quater, P.B. (2015), Planning for PV plant performance monitoring by means of unmanned aerial systems (UAS), *International Journal of Energy and Environmental Engineering*, Vol. 6, No. 1, pp. 47-54.

Kim, D., Youn, J., and Kim, C. (2016a), Determination of defective photovoltaic module by using thermography, *Proceedings of the 37th Asian Conference on Remote Sensing (ACRS)*, 17-21 October, Colombo, Sri Lanka.

Kim, D., Youn, J., and Kim, C. (2016b), Automatic photovoltaic panel area extraction from uav thermal infrared images, *Journal of the Korean Society of Surveying, Geodesy, Photogrammetry and Cartography*, Vol. 34, No. 6, pp. 559-568.

Köntges, M., Kurtz, S., Packard, C., Jahn, U., Berger, K.A., Kato, K., Friesen, T., Liu, H., Iseghem, M.V., Wohlgemuth, J., Miller, D., Kempe, M., Hacke, P., Reil, F., Bogdanski, N., Herrmann, W., Buerhop-Lutz, C., Razongles, G., and Friesen, G. (2014), *Review of Failures of Photovoltaic Modules*, Report IEA-PVPS T13-01:2014, International Energy Agency Photovoltaic Power Systems Programme (IEA-PVPS), Switzerland, pp. 33-35.

McGlone, J.C., Mikhail, E.M., and Bethel, J.S. (2004), *Manual of Photogrammetry*, American Society of Photogrammetry and Remote Sensing, pp. 969-970.

Quater, P.B., Grimaccia, F., Leva, S., Mussetta, M., and Aghaei, M. (2014), Light Unmanned Aerial Vehicles (UAVs) for Cooperative Inspection of PV Plants, *IEEE Journal of Photovoltaics*, Vol. 4, No. 4, pp. 1107-1113.

Rogotis, S., Ioannidis, D., Tsolakis, A., Tzovaras, D., and Likothanassis, S. (2014), Early defect diagnosis in installed PV modules exploiting spatio-temporal information from thermal images, *Proceedings of the 12th Quantitative InfraRed Thermography Conference (QIRT)*, 7-11 July, Bordeaux, France.

Shin, W.-G., Jung, T.-H., Go, S.-H., Ju, Y.-C., Chang, H.-S., and Kang, G.-H. (2015), Analysis of thermal & electrical characteristics variation of PV module with damaged bypass diodes, *Journal of the Korean Solar Energy Society*, Vol. 35, No. 4, pp. 67-75.

Tsanakas, J.A., Chrysostomou, D., Botsaris, P.N., and Gasteratos, A. (2015), Fault diagnosis of photovoltaic modules through image processing and Canny edge detection on field thermographic measurements, *International Journal of Sustainable Energy*, Vol. 34, No. 6, pp. 351-372.